Robotica: (2021) volume 39, pp. 2153–2171. © The Author(s), 2021. Published by Cambridge University Press.
doi:10.1017/S0263574721000230

Enhanced Dynamic Capability of Cable-Driven Parallel Manipulators by Reconfiguration

Rajesh Kumar* and Sudipto Mukherjee

Mechanical Engineering Department, Indian Institute of Technology Delhi, II-420, Mechatronics Lab, Delhi 110016, India
E-mail: sudipto@mech.iitd.ac.in

(Accepted February 4, 2021. First published online: March 16, 2021)

SUMMARY
Cable-driven parallel manipulators (CDPMs) offer advantages over traditional parallel manipulators. Though their ability to accelerate is higher than the traditional motion platforms, the capabilities are often not used optimally. The issues of cable slackening (especially at higher accelerations) and the emergence of singularity poses have traditional limitations. This paper analyzes and generates manipulator configurations that reduce the effect of these two essential hindrances of deploying CDPMs. A methodology, inspired by rigid body dynamics of multiple contact problems, used to optimize the positions of attachment points, is shown to be effective.

Nomenclature

Symbol	Name
η	Set containing poses in wrench closure workspace
ζ	Set containing poses in wrench feasible workspace
$\mathbf{M}$	Mass matrix of the moving platform
$\{G\}$	Fixed frame attached to the ground
$\{B\}$	Fixed frame attached to the body of the moving manipulator
$\mathbf{a^G}$	Acceleration of the moving platform in the ground frame
$\mathbf{g^G}$	Acceleration due to gravity, written in the ground fixed frame
$\mathbf{w}$	External wrench applied to the moving platform, written in the ground frame
$\mathbf{I_o^G}$	Moment of inertia of the moving platform written in the ground fixed 'G' frame
$\boldsymbol{\alpha^G}$	Angular acceleration of the moving platform written in 'G' frame
$\boldsymbol{\omega^G}$	Angular velocity of the moving platform written in 'G' frame
$\mathbf{W_{net}}$	Net wrench on the moving platform
$\mathbf{J_F}$	Force Jacobian for the moving platform
$\mathbf{\Phi_i}$	ith null space basis vector of J_F matrix
α_i	Coefficient term of $\mathbf{\Phi_i}$
$\mathbf{\Delta}$	Vector containing the tension value for each cable
$\mathbf{f}$	External force on the moving platform
$\mathbf{t}$	External moment on the moving platform
T_i	Tension in the ith cable
$T_{\max}$	Maximum tension in the cable
$\widehat{\mathbf{T}}_\mathbf{i}$	Force vector applied at each mounting point of moving platform, written in the 'G' frame

* Corresponding author. E-mail: rajeshkr96@gmail.com

https://doi.org/10.1017/S0263574721000230 Published online by Cambridge University Press

$\mathbf{T}$	The tension vector containing the $\widehat{\mathbf{T}}_\mathbf{i}$ elements
$\mathbf{r}_\mathbf{k}^\mathbf{G}$	Radius vector from the center of moving platform to the kth mounting point, written in the 'G' frame
$\widetilde{\mathbf{r}}_\mathbf{k}^\mathbf{G}$	Cross-product matrix for the '$\mathbf{r}_\mathbf{k}^\mathbf{G}$' vector
$\mathbf{P}$	Grasp – like matrix for cable-driven robot
$\mathbf{P}^+$	Pseudo-inverse matrix corresponding to a matrix $\mathbf{P}$
$\mathbf{j}_\mathbf{i}$	Null space basis vector corresponding to matrix $\mathbf{P}$
γ_i	Coefficients corresponding to the null space basis vector $\mathbf{j}_\mathbf{i}$
β_i	Coefficient of the direction vector of the kth cable
$\widehat{\boldsymbol{\nu}}_\mathbf{k}^\mathbf{G}$	Direction vector of the kth cable written in ground frame $\{G\}$
$\widehat{\mathbf{k}}_\mathbf{k}$	Derived vector from $\widehat{\boldsymbol{\nu}}_\mathbf{k}^\mathbf{G}$ for the kth cable
$\widehat{\mathbf{i}}, \widehat{\mathbf{j}}, \widehat{\mathbf{k}}$	Direction vectors along orthogonal directions
d_{ij}	The unsigned distance of the jth point of $\{\$_i\}$ from the ith plane in $\{S\}$
$\{\Omega\}$	Set of mounting points on the manipulator
$\{S\}$	Set of planes formed by any three of eight mounting points on the manipulator
$\{\$_i\}$	Instantaneous set of points in $\{\Omega\}$ which do not lie in the ith plane of $\{S\}$
$\mathbf{N}$	Matrix containing null space basis vectors of matrix $\mathbf{P}$
$\mathbf{N'}$	Reformulated form of the matrix $\mathbf{N}$
$\mathbf{E}$	The matrix containing the $\widehat{\mathbf{k}}_\mathbf{k}$ vectors
$\mathbf{H}$	Matrix synthesized by concatenating $\mathbf{N}$ and $\mathbf{E}$ matrices
$\mathbf{m}$	Column containing the β_i and γ_i terms
$\mathbf{l}_\mathbf{ij}^\mathbf{k}$	Formulation used in $\mathbf{N'}$ matrix. If $k = i$ or j , then the vector represents the line joining ith and jth contact, otherwise equal to $\mathbf{0}$ vector
a_i	Variable perturbation along the ith direction
$\mathbf{I}$	Identity matrix

1. Introduction

Cable-driven parallel manipulators (CDPMs)[1] are a relatively new paradigm in the field of motion platforms where the moving platform is attached to the frame with actuated cables. Change of length of the cables leads to a change in the pose of the moving platform. The winch motors actuating the cables are placed on a fixed base frame.[2] The other ends of the cables are attached to the manipulator (Fig. 1).

The unique selling point of CDPMs derives from their moving inertia being significantly lower when compared to the traditional parallel robots and tolerance to assembly and manufacturing. These robots are used in high-speed manipulation applications.[3] Given the high scalability of the manipulator, the CDPMs are placed at large construction sites.[4–6] The CDPMs are also used in neurorehabilitation (like NeReBot,[7] waist rehabilitation robot[8]), large-scale 3D Printing[9–12] and search-and-rescue operations.[13] As the cable-driven robots have small moving inertia, haptic interfaces have been developed using them.[14,15] Modular cable-driven parallel robots have also been synthesized.[16] The cable-driven robots are also used for mounting cameras to cover events,[17,18] as they can map large areas. As CDPMs can gain high acceleration in limited power, they are also useful as motion simulators. Numerous methods have been developed for optimal trajectory planning of CDPMs.[19] For instance, a B-spline architecture was developed by Qian et al.[20] Researchers have also focused on planning and control of CDPMs with flexible cables.[21] For all the considerations, maintain positive tension and avoidance of singular positions are two of the fundamental concerns in different schemes developed.[22–24]

One of the primary concerns with deploying CDPMs is the presence of singularities within the workspace and cable slackening. The existence of singularities within the workspace leads to kinematic indeterminacy and loss of controllability of the manipulator. At a particular singular pose, the available workspace to the manipulator is also reduced. Apart from avoiding the singular poses within the manipulator's workspace, another critical concern is maintaining positive tension in the cables.[25–27]

https://doi.org/10.1017/S0263574721000230 Published online by Cambridge University Press

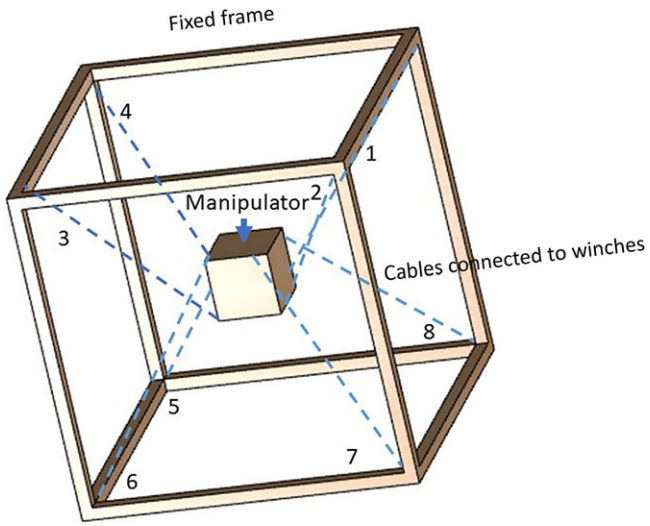


Fig. 1. A cable-driven parallel manipulator kinematic structure with a floating cube as the manipulator and the corners of the fixed frame being the positions of the winches.

The two essential concerns relating to the CDPMs have been dealt with over the years. To improve the workspace usually, a larger number of cables are utilized. The redundancy allows more options while distributing the tension forces to the cables. It is known that for the case of taut CDPMs, the cables can only sustain forces in one direction (tensile forces). It is also known that to constrain an *n dof* system under a fixed external wrench, the minimum number of cables required is n+1.[28] So, even for a known fixed external wrench, a CDPM needs to have single-order redundancy. A reader without a background in the field of screw theory can relate to "wrench" as a combination of forces and moments. It is also known that if the n cables have an arbitrary arrangement, the position of attachment and alignment of the $(n + 1)$th cable is determined by the attachment points and direction of the tension of the other cables. So, the cable-driven parallel robots are developed with a higher number of cables.

Numerous aspects usually describe a kinematic design of the CDPM, including the mounting points on the fixed frame, the mounting points on the moving frame and the number of cables. The unique description of the cable-driven parallel robot results in a particular kinematic behavior of the robot. The manipulator design also describes the available workspace[29–35] to the end-effector of the manipulator.[36] Alternate methodologies have been developed[22–27] to establish the workspace of cable-driven manipulators. Numerous optimization functions have also been deployed to improve the workspace of cable-driven manipulator systems[37,38] for specific use cases. Different optimization techniques have applied to planar cable robots[39–41] as well as the spatial cable robots.[42–44] Methods have been proposed to perform topological as well as dimensional synthesis of cable-driven parallel robots.[45]

Apart from increasing the workspace, the poses of singularity[46] need to be managed while developing the kinematic structure of the CDPM. As the cable-driven robots are designed for high-speed maneuvers,[47] large singularity-free workspaces are useful. Hence, the synthesis of singularity avoidance is a crucial aspect of the design of cable-driven parallel robots. Singularities are known to affect the behavior of cable-driven parallel robots critically. For instance, asymmetric eight cables, *cuboid in cube manipulator* being singular at the center of the fixed frame (symmetric pose)[48] make the robot challenging to be controlled near the center of the fixed frame (a pose which is highly desirable to be achieved for the robot). The paper focuses on improving the singularity-free workspace of a CDPM. A mathematical similarity between cable-driven robots and walking/grasping robots is also demonstrated.

Other instance is shown in this paper, where some critical symmetric poses are not achievable for trivial designs of the manipulators. We show that the *cubic end-effector* (placed in a cubic fixed frame), when manipulated from a cable attached to its corners, does not have a significant singularity-free workspace at all. The *cube in cube manipulator* with winches mounted on cube's vertices is known to be affected by kinematic singularities at numerous poses within its workspace. The centered

https://doi.org/10.1017/S0263574721000230 Published online by Cambridge University Press

cube (all cables of equal length) is a pose of singularity. Hence, practical designers avoid such designs of CDPMs. Hence, this paper focuses on the heuristic that the mounting points can be perturbed to augment the singularity-free workspace.

The improvement is made through a reconfiguration of the cable attachment points on the moving platform. The null space is utilized to enhance the manipulator's capability to resist external wrenches and avoid singularities.

The specification of a workspace is a set of pose vectors along with the acceleration characteristics of the CDPMs. The "Wrench Closure" workspace ζ is defined as a set of poses for which no cable holding onto the platform slackens under *any* external wrench applied to the platform. The "Wrench Feasible" workspace $\eta \subset \zeta$ is a set of poses where the cables holding onto the platform do not slacken for a specified range of wrenches applied at the end-effector. The term "wrench" here refers to a set of forces and torques and is used in screw theory-based robotics.[49] It is known that the IPaNema system[50] has limited wrench closure capabilities, which restricts its use as a simulator to the acceleration of the order of 8–13 g.[51]

With the optimized mounting points proposed here, one can increase the *Wrench Closure Workspace of cube in cube systems*. The proposed method results in a modified geometry of the end-effector, where the *cube in cube system* is free of singularities. The optimization technique removes the singular poses for cuboid in cube systems. We demonstrate that the method proposed when applied to known CDPMs such as the IpaNema robot[50] and Cogiro robot,[52] improves their wrench closure capabilities as well.

2. Mathematical Model of the Manipulator

Two cubics describe the system's geometry (Fig. 1), one fixed and another floating on cables (the manipulator). Initially, the cable mounting points are symmetrically arranged on the fixed as well as the moving frame. The manipulator (or the end-effector) has six degrees of freedom in its workspace. Eight cables hold the moving platform (manipulator). The system has two degrees of redundancy.

We denote the frame $\{B\}$ to be attached to the manipulator (geometric center of the moving cube). The fixed frame, denoted by $\{G\}$, is attached to the geometric center of the fixed cube. Following the Newton–Euler formulation, Eq. (1) defines the dynamics' equations of motion for the end-effector.

$$\underbrace{\begin{pmatrix} \mathbf{M}\mathbf{a}^{G}\text{-}\mathbf{M}\mathbf{g}^{G} \\ \mathbf{I}_{\mathbf{O}}^{\mathbf{G}}\boldsymbol{\alpha}^{\mathbf{G}}+\boldsymbol{\omega}^{\mathbf{G}}\times\mathbf{I}_{\mathbf{O}}^{\mathbf{G}}\boldsymbol{\omega}^{\mathbf{G}} \end{pmatrix}}_{\mathbf{W}_{\mathbf{net}}} - \mathbf{w} = \mathbf{J}_{\mathbf{F}}\boldsymbol{\Delta} \tag{1}$$

where "$\mathbf{J_F}$" is the Force Jacobian matrix, the cable tension vector "$\boldsymbol{\Delta}$ " belongs to $\mathbb{R}^8$, "$\mathbf{M}$" is the mass of the manipulator, $\mathbf{a^G}$ is the acceleration of the manipulator with respect to the $\{G\}$ frame and $\mathbf{g^G}$ is the acceleration due to gravity. The angular acceleration of the manipulator is $\boldsymbol{\alpha}^{\mathbf{G}}$ and $\boldsymbol{\omega}^{\mathbf{G}}$ is the angular velocity of the manipulator. $\mathbf{I}_{\mathbf{O}}^{\mathbf{G}}$ is the moment of inertia tensor of the cube concerning the center of the manipulator (O), and $\mathbf{w}$ is the external wrench applied to the platform. Throughout, we shall use superscript $\{G\}$ to denote representation in $\{G\}$ frame. The force Jacobian matrix relates the forces and wrenches at the end-effector (manipulator) to the tension magnitude at the cables.

The force Jacobian matrix ($\mathbf{J_F}$) is defined using vectors aligned to the cables (Eq. (2)). The terminology in Eq. (2) is shown schematically in Fig. 2.

$$\mathbf{J}_{\mathbf{F}} = \begin{Bmatrix} \mathbf{v}_{\mathbf{1}}^{\mathbf{G}} & \mathbf{v}_{\mathbf{2}}^{\mathbf{G}} & \mathbf{v}_{\mathbf{3}}^{\mathbf{G}} & \mathbf{v}_{\mathbf{4}}^{\mathbf{G}} & \mathbf{v}_{\mathbf{5}}^{\mathbf{G}} & \mathbf{v}_{\mathbf{6}}^{\mathbf{G}} & \mathbf{v}_{\mathbf{7}}^{\mathbf{G}} & \mathbf{v}_{\mathbf{8}}^{\mathbf{G}} \\ \mathbf{r}_{\mathbf{1}}^{\mathbf{G}}\times\mathbf{v}_{\mathbf{1}}^{\mathbf{G}} & \mathbf{r}_{\mathbf{2}}^{\mathbf{G}}\times\mathbf{v}_{\mathbf{2}}^{\mathbf{G}} & \mathbf{r}_{\mathbf{3}}^{\mathbf{G}}\times\mathbf{v}_{\mathbf{3}}^{\mathbf{G}} & \mathbf{r}_{\mathbf{4}}^{\mathbf{G}}\times\mathbf{v}_{\mathbf{4}}^{\mathbf{G}} & \mathbf{r}_{\mathbf{5}}^{\mathbf{G}}\times\mathbf{v}_{\mathbf{5}}^{\mathbf{G}} & \mathbf{r}_{\mathbf{6}}^{\mathbf{G}}\times\mathbf{v}_{\mathbf{6}}^{\mathbf{G}} & \mathbf{r}_{\mathbf{7}}^{\mathbf{G}}\times\mathbf{v}_{\mathbf{7}}^{\mathbf{G}} & \mathbf{r}_{\mathbf{8}}^{\mathbf{G}}\times\mathbf{v}_{\mathbf{8}}^{\mathbf{G}} \end{Bmatrix} \tag{2}$$

where $\mathbf{v}_{\mathbf{i}}^{\mathbf{G}}$ is the vector representing the direction of the cable connected to the ith mounting point of manipulator and $\mathbf{r}_{\mathbf{i}}^{\mathbf{G}}$ is the radius vector to the mounting point from the center of the manipulator (written in the fixed frame, $\{G\}$). The tension vector (Eq. (3)) contains eight elements corresponding

https://doi.org/10.1017/S0263574721000230 Published online by Cambridge University Press

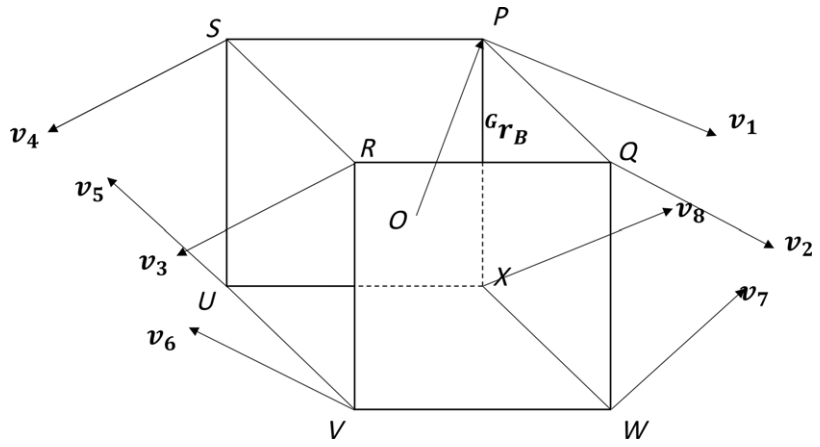


Fig. 2. Radius and tension vectors for mounting points at the vertices of cube.

to the 8×1, and the external wrench in Eq. (1) is

$$\mathbf{\Delta} = (T_i)_{i=1-8} \tag{3}$$

$$\mathbf{w}= \begin{pmatrix} \mathbf{f} \\ \mathbf{t} \end{pmatrix} \tag{4}$$

where $\mathbf{f}$ is the external force on the manipulator, and $\mathbf{t}$ is the external moment on the manipulator, reduced to the origin of the $\{G\}$ frame.

During manipulation of the platform, all the cables need to be taut. A feasible solution to matrix Eq. (1) (which is an underconstrained set) is obtained when all cables are taut. The lower limit on tension is hence zero, and the upper limit to tension is the operational limit of cables, generating another constraint (Eq. (5)).

$$0 \leq T_i \leq T_{\max} \; \forall \; i = 1:8 \tag{5}$$

As T_{max} can be manipulated to large values by using multiple twisted strands and choice of material, we shall limit the discussion only to a kinematic treatment utilizing the lower limit, $T_i \geq 0$.

3. Equivalence of Cable and Contact Manipulated Rigid Body Dynamics

When the manipulator is at a non-singular pose (the pose where all the degrees of freedom of the end-effector are controllable), the Jacobian matrix ($\mathbf{J_F}$) (size: 6×8) has rank 6. Hence, the dynamics of the manipulated cube is deterministic, given the tension values. It means that the motion of the manipulated cube can be predicted if the tension values are known at the cables. On the other hand, the solution for the cable tensions, given a manipulator trajectory, is not unique. The solution of the tension vector $\mathbf{\Delta}$ (Eqs. (6)–(8)), for any set of external ($\mathbf{w}$) and body wrenches (acceleration terms), is written as in Eqs. (6)–(8).

$$\mathbf{\Delta} = \mathbf{J_F^+}\,(\mathbf{W_{net}}) + \alpha_1 \mathbf{\Phi_1} + \alpha_2 \mathbf{\Phi_2} \tag{6}$$

$$\mathbf{\Delta_1} = \mathbf{J_F^+}\,(\mathbf{W_{net}}) \tag{7}$$

$$\mathbf{\Delta_2} = \alpha_1 \mathbf{\Phi_1} + \alpha_2 \mathbf{\Phi_2} \tag{8}$$

where $\mathbf{J_F^+}$ is the Moore Penrose pseudo-inverse[57] of the force Jacobian matrix ($\boldsymbol{J}_F$) and '$\mathbf{\Phi_1'}$ and '$\mathbf{\Phi_2'}$ are unit-norm, independent, column basis vectors of the resulting 2D null space of the force Jacobian matrix ($\mathbf{J_F}$). Independent basis vectors are orthogonal to one another. $\mathbf{W_{net}}$ represents the left-hand side vector in Eq. (1).

The proposed architecture in Eqs. (6)–(8) is similar to the null space assignment method, which is popular for the cases of walking robots and dextrous fingers.[53] However, for the latter two cases, the allowable forces at the attachment points for CDPMs are more restrictive. While contact forces can be multidirectional (limited to the friction cone) for grasping and walking, the direction of forces applied to the end-effector of CDPMs is *strictly* along the direction of the cables. Consequently, the

https://doi.org/10.1017/S0263574721000230 Published online by Cambridge University Press

traditional method of representing the dynamics of the cable-driven manipulator (Eqs. (6)–(8)) does not provide full information about the nature of the forces. We know that for similar systems where *contact forces* are applied to the object at multiple points, the force distribution is generated from two underlying force fields. One is the equilibrating force field, and the other is the interaction force field (corresponding to the null space solution).[57]

A force vector is said to belong to equilibrating force field if its application results in a net motion of the object, whereas a force vector is said to belong to the interaction force field if it is non-trivial and does not result in motion of the object, that is, belongs to the null space solution. Throughout this paper, the "interaction field" refers to the forces generated from null space solutions. Eqs. (6)–(8) do not provide an interpretation of forces as belonging to either of the fields. Equilibrating force field and interaction force fields correspond to the distribution of force vectors. We note that Eqs. (6)–(8) provide the distribution of a set of tension magnitudes (pre-defined directions). Hence, we need to reformulate the distribution of forces to effectively utilize the ideas of equilibrating and interaction force fields of contact-induced forces. The use of term field as opposed to vector is due to the presence of underlying geometries like helicoids, which can be defined compactly based on the set of contact points, which in turn generate the corresponding force vectors. It suffices to use the "field" as nomenclature as we shall not require computation of the underlying geometry in this treatment.

This paper focuses on redesigning the mounting points on the end-effector to ensure that the forces belonging to the interaction field are utilized optimally. We, then, reformulate the instantaneous dynamics of cable-driven parallel robots to analyze the geometric characteristics of the equilibrating and interaction force fields using the set of Eqs. (9)–(16).

To reformulate the governing equations of the distribution of tension vectors, we first assume that the generalized contact forces are applied at the point of attachment (hence, forming a vector field) and then impose the constraint that the direction of the contact forces should be coincident to the vector describing the cable direction. We assume general contact forces $\widehat{\mathbf{T}}_\mathbf{i}$ to be applied at each contact points. The architecture results in:

$$\underbrace{\begin{bmatrix} \mathbf{I} & \mathbf{I} & \mathbf{I} & \mathbf{I} & \mathbf{I} & \mathbf{I} & \mathbf{I} & \mathbf{I} \\ \widetilde{\mathbf{r}}_\mathbf{1}^\mathbf{G} & \widetilde{\mathbf{r}}_\mathbf{2}^\mathbf{G} & \widetilde{\mathbf{r}}_\mathbf{3}^\mathbf{G} & \widetilde{\mathbf{r}}_\mathbf{4}^\mathbf{G} & \widetilde{\mathbf{r}}_\mathbf{5}^\mathbf{G} & \widetilde{\mathbf{r}}_\mathbf{6}^\mathbf{G} & \widetilde{\mathbf{r}}_\mathbf{7}^\mathbf{G} & \widetilde{\mathbf{r}}_\mathbf{8}^\mathbf{G} \end{bmatrix}}_{\mathbf{P}} \underbrace{\begin{bmatrix} \widehat{\mathbf{T}}_\mathbf{1} \\ \widehat{\mathbf{T}}_\mathbf{2} \\ \widehat{\mathbf{T}}_\mathbf{3} \\ \widehat{\mathbf{T}}_\mathbf{4} \\ \widehat{\mathbf{T}}_\mathbf{5} \\ \widehat{\mathbf{T}}_\mathbf{6} \\ \widehat{\mathbf{T}}_\mathbf{7} \\ \widehat{\mathbf{T}}_\mathbf{8} \end{bmatrix}}_{\mathbf{T}} = \mathbf{W_{net}} \tag{9}$$

where $\widehat{\mathbf{T}}_\mathbf{i} = \begin{bmatrix} T_{i,x} \\ T_{i,y} \\ T_{i,z} \end{bmatrix}$ represents arbitrary vectors in each direction, $\widetilde{\mathbf{r}}_\mathbf{k}^\mathbf{G}$ represents the cross-product matrix corresponding to the vector $\mathbf{r}_\mathbf{k}^\mathbf{G}$ for the kth mounting point. A cross-product matrix corresponding to vector $\mathbf{v}$ is given as $\begin{bmatrix} 0 & -v_z & v_y \\ v_z & 0 & -v_x \\ -v_y & v_x & 0 \end{bmatrix}$, where v_x, v_y, and v_z are the three orthogonal components of the vector (x, y, z, respectively).

We, however, know that each of the net tension vector $\widehat{\mathbf{T}}_\mathbf{i}$ should physically lie along the vector along which cable is stretched. The generalized solution of Eq. (9) results in:

$$\mathbf{T} = \underbrace{\mathbf{P^+ W_{net}}}_{\substack{\text{Force Vectors leading} \\ \text{to Equilibrating field}}} + \underbrace{\sum_{i=1}^{18} \gamma_\mathbf{i} \mathbf{j_i}}_{\substack{\text{Force Vectors leading} \\ \text{to Interaction force field}}} \tag{10}$$

https://doi.org/10.1017/S0263574721000230 Published online by Cambridge University Press

where γ_i is a scalar and $\mathbf{j_i}$ corresponds to ith basis vector of the null space of the matrix **P**. The null space basis vectors are of the unit norm, orthogonal to one another and space the null space of the matrix **P.** Equation (10) suggests the distribution of force vectors (each 3-dimensional vector contained in **T**). Hence, the concept of equilibrating and interaction force fields as in contact forces may be used. Equation (11) states that the combination of force vectors belonging to the interaction force field and the equilibrating field should result in vectors aligned with the cable directions.

$$\mathbf{P^{+}W_{net}} + \sum_{i=1}^{18} \gamma_i \mathbf{j_i} = \begin{pmatrix} \beta_1 \widehat{\boldsymbol{\nu}_1^{\mathbf{G}}} \\ \beta_2 \widehat{\boldsymbol{\nu}_2^{\mathbf{G}}} \\ \beta_3 \widehat{\boldsymbol{\nu}_3^{\mathbf{G}}} \\ \beta_4 \widehat{\boldsymbol{\nu}_4^{\mathbf{G}}} \\ \beta_5 \widehat{\boldsymbol{\nu}_5^{\mathbf{G}}} \\ \beta_6 \widehat{\boldsymbol{\nu}_6^{\mathbf{G}}} \\ \beta_7 \widehat{\boldsymbol{\nu}_7^{\mathbf{G}}} \\ \beta_8 \widehat{\boldsymbol{\nu}_8^{\mathbf{G}}} \end{pmatrix} \tag{11}$$

Equation (11) is a system of 24 equations in 26 variables, reformulated in matrix form in Eq. (12). Since the interaction force field does not affect the manipulator dynamics, we can assign interaction forces such that the tension vectors are directed along the length of the cables. This reassignment creates a solution that is both physically and algebraically consistent.

$$\underbrace{\left(\underbrace{\mathbf{j_1} \; \ddots \; \mathbf{j_{18}}}_{\mathbf{N}} \; \Big| \; \underbrace{\widehat{\mathbf{-k_1}} \; \ddots \; \widehat{\mathbf{-k_8}}}_{\mathbf{E}} \right)}_{\mathbf{H}} \underbrace{\begin{pmatrix} \gamma_1 \\ \vdots \\ \gamma_{18} \\ \beta_1 \\ \vdots \\ \beta_8 \end{pmatrix}}_{\mathbf{m}} = -\mathbf{P^{+}W_{net}} \tag{12}$$

where $\widehat{\mathbf{k_i}} = \begin{pmatrix} \mathbf{0_{3i\text{-}3\times 1}} \\ \widehat{\boldsymbol{\nu}_{\mathbf{i}}^{\mathbf{G}}} \\ \mathbf{0_{24\text{-}3i\times 1}} \end{pmatrix}$. For instance, the first column of matrix **E** becomes: $\widehat{\mathbf{k_1}} = \begin{pmatrix} \widehat{\mathbf{v_1^G}} \\ \mathbf{0_{21\times 1}} \end{pmatrix}$, the second column as $\widehat{\mathbf{k_2}} = \begin{pmatrix} \mathbf{0_{3\times 1}} \\ \widehat{\mathbf{v_2^G}} \\ \mathbf{0_{18\times 1}} \end{pmatrix}$ and the eighth column as $\widehat{\mathbf{k_8}} = \begin{pmatrix} \mathbf{0_{21\times 1}} \\ \widehat{\mathbf{v_8^G}} \end{pmatrix}$

A set of constraints needs to be applied to Eq. (11). The constraints imply that the tension vectors are directed along the cable vectors. After applying the constraints, the matrix **H** takes the form as in Eq. (12). The components of **H** comprise of the set containing the null space basis (**N**) vectors. The matrix **N** is computed using the method presented in ref. [59]. The matrix **N** (comprising of vectors resulting in the interaction force field) can be spanned entirely from equal and opposite vectors joining the mounting points. Hence, the matrix **N** is computable knowing the kinematic state of the system. Equation (12) is a transformation of Eq. (1). Equation (1) is obtained by premultiplying both sides of Eq. (12) with the CDPM grasp matrix (**P**) (Eqs. (13)–(16)). Multiplying the "−**P**" matrix on both sides, we get

https://doi.org/10.1017/S0263574721000230 Published online by Cambridge University Press

$$-\mathbf{PH}\underbrace{\begin{pmatrix}\gamma_1\\ \vdots\\ \gamma_{18}\\ \beta_1\\ \vdots\\ \beta_8\end{pmatrix}}_{\mathbf{m}}=\mathbf{PP^{+}W_{net}} \tag{13}$$

For all null space basis vectors, we know that $\mathbf{Pj_i}=[\mathbf{0}]\ \forall\ i=1:18$. Also, to compute **PE**, we use the notations as:

$$-\mathbf{PH}=[\mathbf{0_{24\times 18}}|-\mathbf{PE}] \tag{14}$$

$$-\mathbf{PE}=-\begin{bmatrix}\mathbf{I} & \mathbf{I} & \mathbf{I} & \mathbf{I} & \mathbf{I} & \mathbf{I} & \mathbf{I} & \mathbf{I}\\ \widetilde{\mathbf{r}_1} & \widetilde{\mathbf{r}_2} & \widetilde{\mathbf{r}_3} & \widetilde{\mathbf{r}_4} & \widetilde{\mathbf{r}_5} & \widetilde{\mathbf{r}_6} & \widetilde{\mathbf{r}_7} & \widetilde{\mathbf{r}_8}\end{bmatrix}\begin{pmatrix}\widehat{\mathbf{-k_1}} & & \\ & \ddots & \\ & & \widehat{\mathbf{-k_8}}\end{pmatrix} \tag{15}$$

$$-\mathbf{PE}=\begin{pmatrix}\mathbf{v_1^G} & \mathbf{v_2^G} & \mathbf{v_3^G} & \mathbf{v_4^G} & \mathbf{v_5^G} & \mathbf{v_6^G} & \mathbf{v_7^G} & \mathbf{v_8^G}\\ \mathbf{r_1^G}\times\mathbf{v_1^G} & \mathbf{r_2^G}\times\mathbf{v_2^G} & \mathbf{r_3^G}\times\mathbf{v_3^G} & \mathbf{r_4^G}\times\mathbf{v_4^G} & \mathbf{r_5^G}\times\mathbf{v_5^G} & \mathbf{r_6^G}\times\mathbf{v_6^G} & \mathbf{r_7^G}\times\mathbf{v_7^G} & \mathbf{r_8^G}\times\mathbf{v_8^G}\end{pmatrix} \tag{16}$$

So, $-\mathbf{PE}=\mathbf{J_F}$, and Eq. (12) reduces to Eq. (1).

We note that Eq. (11) is structurally similar to Eq. (1). We can associate the mathematics of the tension distribution problem in CDPM to that of grasping and other multi-contact problems. Equation (11) suggests that a portion of the interaction force field (Null space solution) is utilized to ensure that the tension vectors are aligned to specific directions. As Eq. (11) is still an underdetermined system, we can utilize the remaining portion of the null space to ensure that the cables are taut. This freedom of degree 2 appears in Eq. (1) as the coefficients of the basis vectors of the 2D null space of a scalar field of tension vectors.

The set of Eqs. (10)–(16) suggests that the case of CDPM has a solution set that is a subset of that of grasping with multiple contacts. The apparent difference is that grasping has allowable forces oriented towards the inward-directed normal while cable-based manipulation has allowable forces aligned to the outward normal. The less noticeable difference is that for CDPMs, a part of the interaction field solution goes into aligning contact forces *strictly* along with cable directions.

The matrix **N** is computed from the vectors joining the mounting points (using the method presented in ref. [23]) in Eq. (12). To calculate the matrix **N**, the matrix **N** is reformulated to a 24×28 matrix with rank 18 ($\mathbf{N}'$). So it still has 18 independent rows. The reformulation allows a closed-form expression of the interaction field solution. We reformulate the null space matrix **N** to $\mathbf{N}'$, with the elements of $\mathbf{N}'$ as shown in Eq. (17).

$$\mathbf{N}'=\begin{Bmatrix}\mathbf{l_{12}^1 l_{13}^1 l_{14}^1}\cdots\mathbf{l_{1m}^1}\ \ \mathbf{l_{23}^1}\cdots\mathbf{l_{2m}^1}\cdots\ \mathbf{l_{m-1,m}^1}\\ \vdots\\ \mathbf{l_{12}^k l_{13}^k l_{14}^k}\cdots\mathbf{l_{1m}^k}\ \ \mathbf{l_{23}^k}\cdots\mathbf{l_{2m}^k}\cdots\ \mathbf{l_{m-1,m}^k}\end{Bmatrix} \tag{17}$$

where "*m*" is the number of contact points. $\mathbf{l_{ij}^k}$ is defined according to the set in Eq. (18).

$$\mathbf{l_{ij}^k}=\begin{cases}\dfrac{\mathbf{r_j^G}-\mathbf{r_i^G}}{||\mathbf{r_i^G}-\mathbf{r_j^G}||} & \text{if}\quad \mathrm{k}=\mathrm{i}\\ \dfrac{\mathbf{r_i^G}-\mathbf{r_j^G}}{||\mathbf{r_i^G}-\mathbf{r_j^G}||} & \text{if}\quad \mathrm{k}=\mathrm{j}\\ \mathbf{0}\ \text{otherwise}\end{cases} \tag{18}$$

So, the column space of the matrix $\mathbf{N}'$ consists of 18 independent vectors for an 8-point contact. The equivalence of the column space of the interaction forces and the null space solution is presented in refs. 59 and 57 for the case of noncoplanar grasps with $m>3$ (m is the number of contact points).

https://doi.org/10.1017/S0263574721000230 Published online by Cambridge University Press

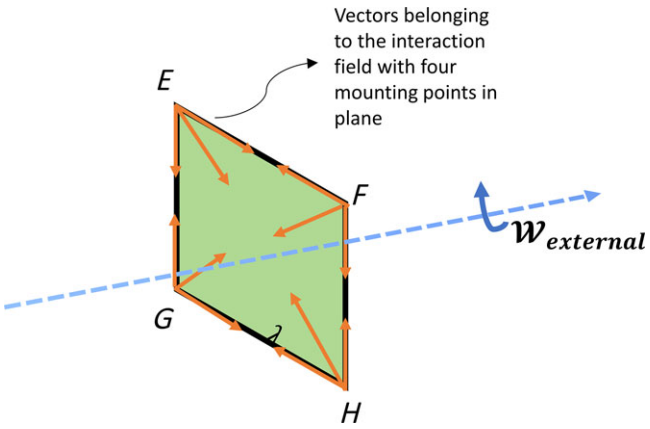


Fig. 3. The interaction force field for a planar manipulator with four in-plane mounting points.

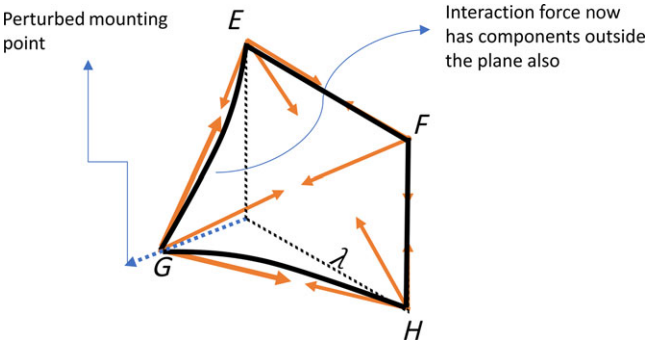


Fig. 4. The perturbation of one mounting point outside the plane improves the interaction force field. The interaction force now can have force components outside the plane λ.

So, the null space matrix **N** in Eq. (12) is synthesized from the basis vectors belonging to the column space of **N**′, which is spanned by the set of vectors aligned with directions obtained by connecting vertices of the moving cube. Noncoplanar grasps relate to the existence of more than three nonplanar contact points.

It is known that the interaction force field is generated by the set of equal and opposite forces acting along the direction connecting the two mounting points. So, the matrix **H** is constructed from a set of vectors joining ends of the mounting points within the cube (**N**′and hence, **N**) and a set of vectors along the tension vectors (**E**). It is observed that the matrix **H** is ill-conditioned for a *cube in cube* manipulator with its mounting points on vertices of the cube (and the center of the end-effector coinciding with that of the fixed structure). The ill-conditioning can be related to the fact that the subspaces formed by the interaction force matrix (**N**) and the constraint matrix due to the tension directions (**E**) form a dependent set. Similar ill-conditioning is classified as type 5b earlier.[58]

4. Design and Analysis of the Optimization Function

We have established that the mathematical formulation for cable robots is equivalent to that of the grasping problems where four planar grasp points create an ill-conditioned interaction force field (Fig. 3). As the four mounting points are planar, the vectors belonging to the interaction field do not have a component orthogonal to the plane. This specific ill-conditioning results in the interaction force field unable to contribute to modifications to the tension solutions. The ill-conditioning occurs because the tension forces require an out-of-plane force contribution. The perturbation of one of the mounting points (Fig. 4) improves the interaction field. Now, the vectors belonging to the interaction force field span the $\mathbb{R}^3$ space.

Although it is not feasible to interpret the eight-dimensional case geometrically, we hypothesize that the singularities lying within the workspace arise from the existence of multiple sets of four coplanar points on the cubical end-effector. A finite perturbation of one point in a direction away

https://doi.org/10.1017/S0263574721000230 Published online by Cambridge University Press

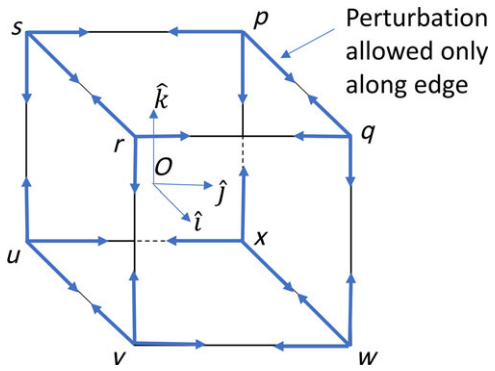


Fig. 5. Constraints for the allowed perturbations of the mounting points for the cube.

from the three nominal planes in Fig. 5 removes the singularity. Correspondingly, a perturbation of one of the mounting points away from the plane containing the other three imparts the interaction force field the ability to provide expected forces. At the nominal position (defined as a pose with the centers of the larger and smaller cube coincident with an orientation such that the inner and outer cubes have all six faces parallel to the large cube), moving every fourth point out of the plane ensures that the type 4d singularity is avoided (as described in the literature[58]).

Since the matrix **P** consists of columns, which are screws, by definition, the same dynamics' equations are generated under change of origin and rotation, corresponding to different positions of the end-effector. Hence, the singularity-free workspace of the symmetric cable-driven manipulator is optimized by manipulating the structure of the **H** matrix alone. The structure of the matrix is changed by perturbing the mounting points on the end-effector.

To improve the singularity-free workspace, we propose minimizing a measure parametrized by perturbating the mounting points from the corner of the cube. In later examples, we shall show that such perturbation removes singularities in the example cases and improves the workspace for cable manipulators with symmetric mounting points.

For eight mounting points on the cube, we can define ${}^8C_3$ planes, each defined by three of the mounting points. We hypothesize that for each of these cases, the remaining five points should be dispersed maximally with respect to any of the ${}^8C_3$ planes created. Consider the *i*th plane created by any three out of the eight points on the manipulator. The other five points should be dispersed to the furthest distance possible from these planes.

The optimization function to capture the dispersion of the mounting points (Eq. (19)) is given by:

$$f(\Omega) = \max\left(\sum\nolimits_{i\in S}\left(\prod\nolimits_{j\in \$_i} \mathrm{d}_{ij}\right)\right) \tag{19}$$

where $\{\Omega\}$ is the set of mounting points on manipulator; $\{S\}$ is the set of planes formed by any three of eight points. $\{\$_i\}$ is the instantaneous set of points in $\{\Omega\}$, which do not lie in the *i*th plane of $\{S\}$. d_{ij} is the unsigned distance of the *j*th point of $\{\$_i\}$ from the *i*th plane in $\{S\}$. The more obvious choice for the functionals, the sum of squared distances, is not preferred as that functional was seen to allow the growth of a few high valued terms.

We could, in general, perturb the corner points over the three adjoining faces. However, mounting the points on the face may not be practical as it can potentially lead to cable engaging with the cube edge. The mounting points are perturbed only along the edges of the cube (Fig. 5). For instance, the perturbation $P_m(\mathbf{p})$ acting on point **p** is given by:

$$P_m(\mathbf{p}) = a_1\hat{\mathbf{i}} - a_2\hat{\mathbf{j}} - a_3\hat{\mathbf{k}} \tag{20}$$

$\forall\, a_1, a_2, a_3 \geq 0$ and only one of the three being nonzero at any instance.

The value of the objective function was computed for all possible combinations of feasible points. The attachment points were perturbed along the edges in steps of 0.025 m (ranging from 0 to 0.5 m). Once the optimum pose was localized (between two steps), the step size was reduced to 0.002 m (to get a better estimate). An exhaustive search method was used to localize the optimal geometry. The exhaustive search utilized all combinations of perturbations of different points along different

https://doi.org/10.1017/S0263574721000230 Published online by Cambridge University Press

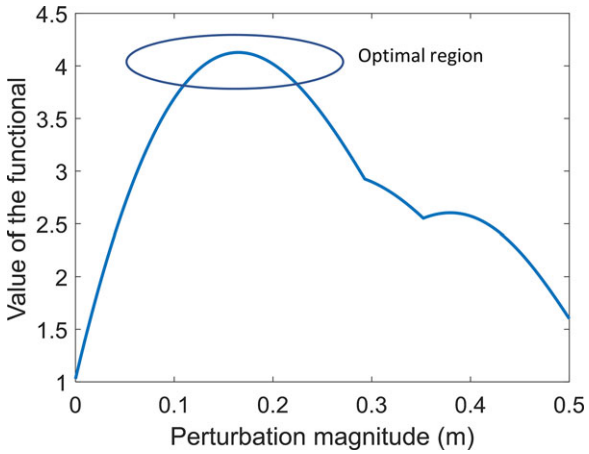


Fig. 6. Variation of the function with an equal excursion on eight vertices (only for the sake of visualization). The simulation, however, covered all possible value sets.

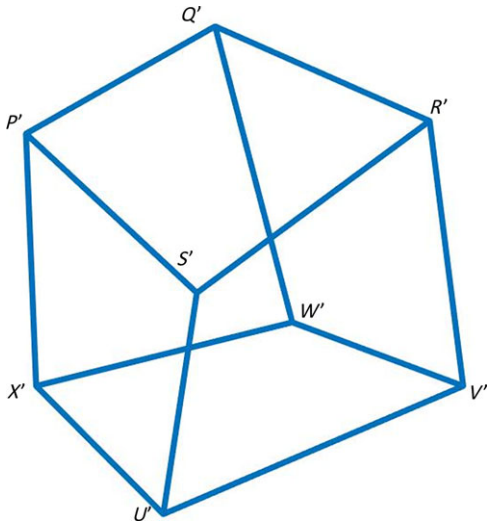


Fig. 7. The geometry of mounting points leading to an optimal characteristic of null space ((**p,q,r,s,u,v,w,x**) get transformed to (**P',Q',R',S',U',V',W',X'**)).

directions. The configuration corresponding to the maximum value of the cost function is presented in Fig. 7. The resulting optimal geometry leads to perturbation of all the eight mounting points being of equal magnitude. For visualization purposes, in Fig. 6, all the attachment points are perturbed by equal magnitude along the edges in steps of 0.002 m from 0.0 to 0.5 m.

The resulting geometry (Fig. 7) obviously ensures that no four points are in a plane.

For a cube of side length unity, Table I shows coordinates of the optimized mounting points in $\{B\}$ frame.

The resulting set of mounting points, leading to the configuration, is shown in Fig. 8.

5. Analysis of the Architecture

The geometry created by perturbing the mounting points on the moving cube along with the symmetry of the fixed frame mounting points has resulted in a partition of the basis vectors of the 2D null space, '$\mathbf{\Phi}_1^{'}$ and '$\mathbf{\Phi}_2$'. The positive and zero terms in the column vector representation of the null space are at alternate positions. This ensures that the two null spaces are complementary to one another.

https://doi.org/10.1017/S0263574721000230 Published online by Cambridge University Press

Table I. Optimized coordinates of mounting points of the cube. Presented for unity dimensions but can be scaled to any size.

Point	**Coordinates**
P'	(−0.5, 0.336, 0.5)
Q'	(0.336, 0.5, 0.5)
R'	(0.5, −0.336, 0.5)
S'	(−0.5, −0.5, 0.336)
U'	(−0.5, −0.336, −0.5)
V'	(0.5, −0.5, −0.336)
W'	(0.5, 0.336, −0.5)
X'	(−0.336, 0.5, −0.5)

Table II. Dimensions of the manipulator to analyze the null space characteristics.

Manipulator characteristic	**Value**
Size of manipulator cube	1 m
Size of frame cube	5 m
Pose 1	[0;0;0;0;0;0]
Pose 2	[0;0;0;20°;20°;20°]
Mass of the end-effector	300 Kg

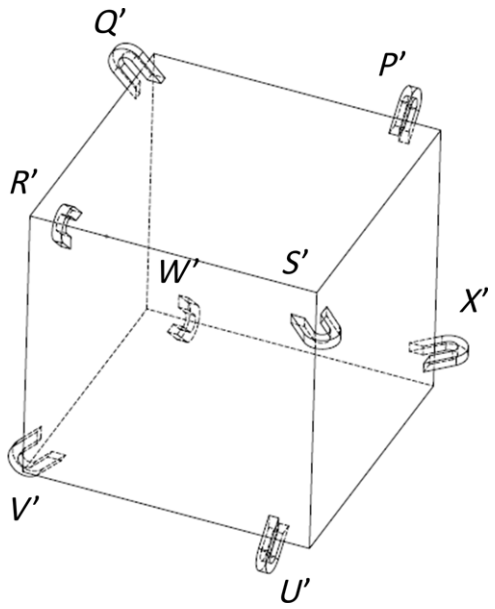


Fig. 8. Positions of mounting points on cube manipulator.

The nature of the null space is independent of the size of the cube ("*a*") and depends only on the relative geometry of attachment points of the cable on the moving cube. The manipulator characteristics in Table II result in the partitioned null space in Table III. The load description, in this case, is of the cube being held at rest by the cables and only the gravitational force acting on the system.

The pose vector consists of the displacement vector (about the $\{G\}$ frame and the rotation about the axis of the $\{G\}$ frame). The moment of inertia tensor was calculated based on the dimensions of the cubical end-effector (assuming a solid cube).

For a change in the angular position of the manipulator (pose 2 in Table) and raising the mass of the end-effector to 600 kg, yet again the inner cube being held stationary under gravity loading, partitioning is visible (Table IV), but the zero elements seen in the nominal case are perturbed. The null space $\mathbf{\Phi_1}$ has all odd elements positive and the magnitudes of even elements are nearly zero.

https://doi.org/10.1017/S0263574721000230 Published online by Cambridge University Press

Table III. Characteristics of null space basis vectors for the position of manipulator at the origin.

S. no	$\mathbf{\Phi_1}$	$\mathbf{\Phi_2}$	$\mathbf{\Delta_1}$ (N)	$\mathbf{\Delta}$ (a possible viable solution) (N)
1	0.5	0.04	1012.51	2707.8
2	−0.04	0.51	−1915.66	513.24
3	0.5	0.04	903.15	2598.44
4	−0.04	0.49	−2078.45	235.08
5	0.5	0.04	−903.15	792.14
6	−0.04	0.49	2078.45	4391.98
7	0.5	0.04	−1012.51	682.78
8	−0.04	0.51	1915.66	4344.56

Table IV. Characteristics of null space basis vectors for the position of manipulator at origin tilted in three directions (position 2 in Table II).

S. no	$\mathbf{\Phi_1}$	$\mathbf{\Phi_2}$	$\mathbf{\Delta_1}$ (N)	$\mathbf{\Delta}$ (a possible viable solution)
1	0.46176	−0.0872	2339.06	3949.79
2	0.08984	0.5326	−3452.43	1257.68
3	0.46114	−0.0857	2145.12	3764.54
4	0.08928	0.5106	−3796.97	734.67
5	0.52704	−0.0339	−1424.36	939.14
6	0.02065	0.4557	4485.29	8234.92
7	0.52843	−0.0324	−1641.83	740.63
8	0.02509	0.4802	4205.89	8173.26

Combined with the symmetry of the "cube in cube" system, the resulting geometry has led to null basis vectors with only a small intersection. In both the examples here and in a host of other cases computed, null space vector $\mathbf{\Phi_2}$ is complementary to $\mathbf{\Phi_1}$ with all odd elements close to zero and even elements positive. The complementary structure of the two null space vectors allows us to generate tension vectors defined according to Eq. (7) (Table III and Table IV) in a computationally efficient manner. In an illustration presented below, the pseudo-inverse solution $\mathbf{\Delta_1}$ has both positive and negative elements. However, as negative elements of $\mathbf{\Phi_1}$ and $\mathbf{\Phi_2}$ are nearly zero, there exist 'α_1' and 'α_2' such that $\mathbf{\Delta_2}$ is a vector with all elements positive. So, the 2D null space allows us to nudge the negative tension elements in $\mathbf{\Delta_1}$ to be positive in $\mathbf{\Delta}$ at the cost of increasing the magnitude of already positive tensions in $\mathbf{\Delta_1}$.

This geometry results in a partitioning of the null spaces. Hence, it allows arbitrarily large external wrenches to be resisted by the system, which translates to the availability of high acceleration to the end-effector cube. The clean partitioning of the null space basis vectors tends to erode as the end-effector cube moves away from the origin of the fixed $\{G\}$ frame. Even then, the geometry created by perturbation of the mounting points ensures that a substantial volume of the fixed cube is available under wrench closure.

The wrench closure workspace (Fig. 9) of the optimized configuration, plotted using the method in ref. [48], has a significant volume around the origin. The workspace created is free of singularities. The method ensures the existence of α_1 and α_2 such that Eq. (7) is satisfied.

The optimization of the attachment point led to an improvement in the volume of the available *wrench-closure* workspace. The wrench closure workspace increases to about 18–20% of the volume of the fixed cube. The resulting workspace allows a translational stroke of around 55% of the length of the side of the fixed cubical frame. For the "cube-in-cube" system, the singularity-free workspace under wrench closure is seen to be more than that typically required for use as a motion platform. The workspace volume refers to the ratio of the volume created by achieved poses vis-à-vis the available poses.

IPaNema vehicle simulator, as described in ref. [50], has a large "wrench feasible" space, but its "Wrench closure workspace" for a constant orientation is small. Though it is a non-symmetric system (i.e., the geometries of the manipulator and the fixed system are not symmetric), the perturbation of mounting points to a noncoplanar attire, based on the method proposed here (Eq. (9)) improves its

https://doi.org/10.1017/S0263574721000230 Published online by Cambridge University Press

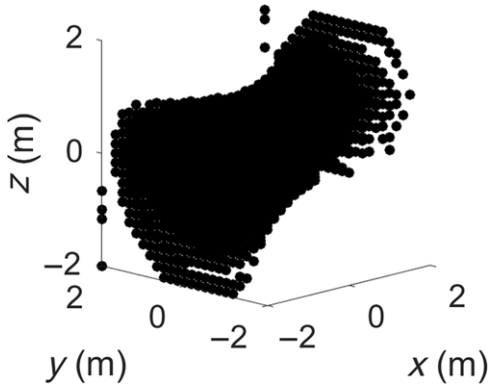


Fig. 9. The wrench closure workspace of the defined geometry at the angular positions of [0°; 0°; 0°].

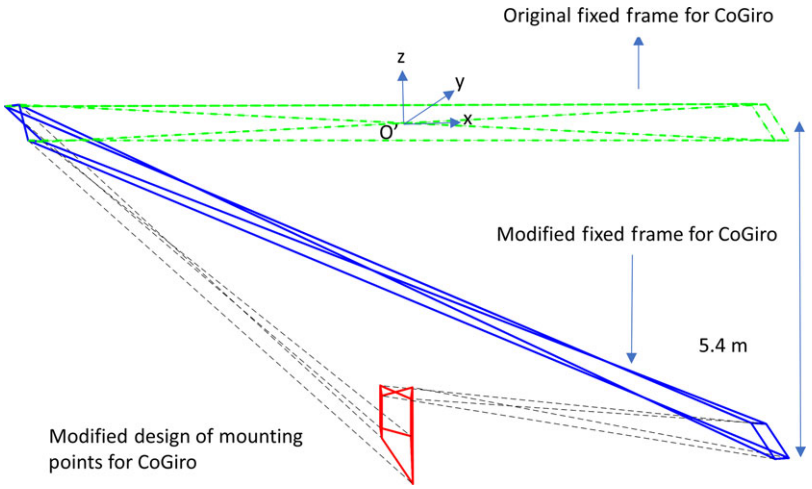


Fig. 10. Proposed redesign for the CoGiro manipulator.

"Wrench-closure capabilities". If we perturb the mounting points based on the function above, the wrench closure workspace volume increases by around 10.2%.

The methodology proposed here is useful only when the wrench closure is not heavily restricted due to the geometry of the fixed-frame mounting points. The CoGiro manipulator[52] has all the eight cables mounted from the top of the frame, and the reorientation of mounting points of the end-effector does not help in improving its capability to restrain a force larger than self-weight directed vertically upwards. So, a wrench closure workspace does not exist for this configuration. In order to improve the workspace, four of the mounting points on the fixed frame are needed to be placed downwards. A perturbation of the mounting points on the fixed frame away along with perturbation of the mounting points on the end-effector (as shown in Fig. 10) creates a constant orientation ([0°, 0°, 0°]) wrench closure workspace of about 30% of the volume of a cube (dimension 5 m × 5 m × 5 m, center at coordinates (0,0,-2.5 m) written in O' frame).

6. Embodiment as a Vehicle and Impact Simulator

Traditional manipulators based on the "Stewart Platform" or "Gough Platform"[54] are used as vehicle simulators. Unoptimized mounting points of manipulators have hindered the usage of CDPM due to limited workspace[55] and the presence of singular positions within the workspace. The suggested manipulator design allows an equivalent embodiment of a CDPM as a vehicle simulator with a more allowable workspace than traditional motion platforms.

The mathematical model of the cube-in-cube systems is extended to cuboidal systems (cuboid in a cuboid with same aspect ratio) without changing the algebraic structure of the Jacobian matrix and hence the nature of 2D null space (Fig. 11). The nature of the null space is independent of the size of

https://doi.org/10.1017/S0263574721000230 Published online by Cambridge University Press

Table V. Characteristics of the vehicle simulator motion platform. The limiting poses and accelerations are stated. The CDPM needs to be checked with the same for a practical embodiment.

Manipulator characteristic	**Value**
Surge (x max)	−0.64m/+0.63 m
Sway (y max)	−0.66m/+0.66 m
Heave (z max)	−0.41 m/+0.41 m
Roll max	−29.2°/29.2°
Pitch max	−28.2°/32.9°
Yaw max	−28.7°/28.7°
Roll velocity max	± 35°/s
Pitch velocity max	± 35°/s
Yaw velocity max	± 40°/s
Max surge acceleration (x max)	7 m/s^2
Max sway acceleration (y max)	7 m/s^2
Max heave acceleration (z max)	10 m/s^2
Max roll acceleration	250°/s^2
Max pitch acceleration	250°/s^2
Max yaw acceleration	500°/s^2
Nominal payload for a vehicle simulator	300 Kg

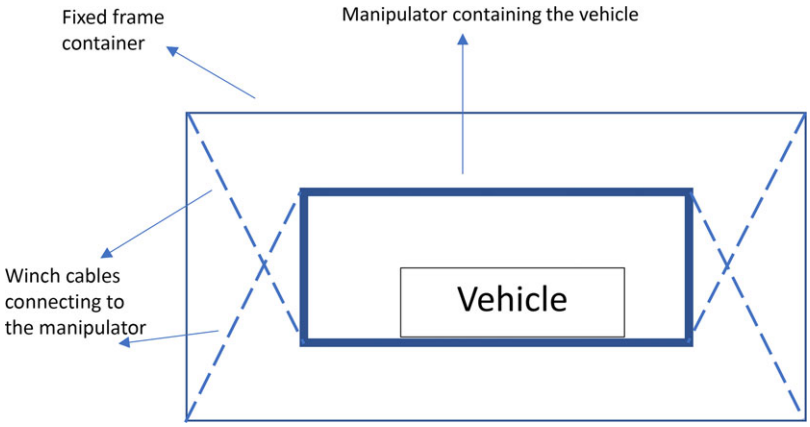


Fig. 11. Embodiment of the system developed as a vehicle simulator. Extended both the manipulator cube and the fixed cube in the length direction, thereby not affecting the Jacobian matrix $\mathbf{J_F}$.

the manipulator so that it can be extended to aircraft simulators as well. The embodiment can handle the typical accelerations required by a vehicle simulator and at extreme angular poses (Table V).

The parameters needed to simulate the vehicle environment is given in Table V.[56] For the band-limited acceleration and angular velocities in a traditional vehicle simulator, the wrench-feasible workspace is relevant. The design with perturbed attachment point allows all required poses, and the wrench-feasible workspace is plotted using the algorithm presented in ref. [35] (Fig. 12).

We study the nature of the null spaces for a nominal payload (300 kg) and a moment of inertia (334.33 kg/m^2). Tables VI-VII show the null vectors, the pseudo-inverse solution vector and one of the "all positive" tension vectors that can be used to control the system at the required acceleration. Table VI presents the behavior of the simulator at the origin with the extreme linear acceleration of {7 m/s^2; 7 m/s^2; 10 m/s^2; 0°/s^2; 0°/s^2; 0°/s^2}.

A solution to the tension vector is shown in column 4 of Table VI. The maximum tension in the cable is around 8.5 kN in order to keep the minimum tension value (133.8 N) positive. The null space basis is visibly partitioned, and they are dependent only on the position of the platform and not applied or body wrenches.

For another test case, with simulator position at an extreme position of workspace, the position vector of {0.64 m; 0.66 m; 0.41 m; 29.2°; 32.9°; 28.7°} and acceleration screw consisting of linear

https://doi.org/10.1017/S0263574721000230 Published online by Cambridge University Press

Table VI. Nullspace characteristics and the required tension vector for the simulator at origin and under the effect of limiting linear acceleration of {7 m/s^2; 7 m/s^2; 10 m/s^2}.

Φ_1	Φ_2	Δ_1 (N)	Δ(a possible viable solution)(N)
0.498	0.04	1464.943	4377.141
−0.041	0.51	−2347.77	2806.2
0.498	0.04	1434.223	4346.422
−0.039	0.486	−4775.84	133.319
0.498	0.04	−2403.28	508.918
−0.039	0.486	3618.046	8527.2
0.498	0.04	−495.886	2416.313
−0.041	0.51	3450.562	8604.533

Table VII. Null space characteristics and the required tension vector for the simulator at pose vector {0.63 m;0.66 m;0.41 m;29.2°;32.9°;28.7°} and under the effect of limiting linear acceleration of {7 m/s^2; 7 m/s^2; 10 m/s^2}.

Φ_1	Φ_2	Δ_1 (N)	Δ(a possible viable solution)(N)
0.462786	−0.04616	271.2238	3304.479
0.085282	0.594481	−1648.5	7604.631
0.484299	−0.02757	295.7609	3769.038
−0.19587	0.397983	−4083.86	88.9842
0.436625	−0.08579	−2252.49	0.231312
−0.03853	0.440149	2608.443	8646.81
0.559601	0.224521	363.7611	8073.607
−0.01915	0.48354	2487.811	9306.684

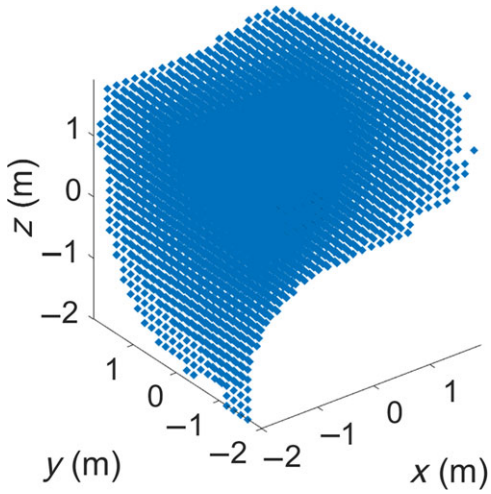


Fig. 12. Workspace plot for one of the limiting poses = [0.63; 0.66; 0.41;29.2°;32.9°;28.7°] and limiting linear acceleration {7 m/s^2; 7 m/s^2; 10 m/s^2}, limiting angular acceleration {250°/s^2; 250°/s^2; 500°/s^2} and angular velocity as in Table V.

acceleration {7 m/s^2; 7 m/s^2; 10 m/s^2; 0°/s^2; 0°/s^2; 0°/s^2} are used. Table VII shows null vectors and a possible solution of tension vector of system. The maximum tension in the cables is around 9.3 kN.

Though the null space basis vectors are less cleanly partitioned at such poses of extreme displacement, they are still assignable to establish the "all positive" tension vectors. The null space basis vectors for all of the extreme cases put together, that is, the simulator under the effect of maximum possible acceleration in the limiting pose is presented in Table VIII.

The peak tension is less than 10 kN, which is easily accommodated by an 8 mm winch cable and demands about two times the peak equilibrating force value. As designed, the manipulator can sustain

https://doi.org/10.1017/S0263574721000230 Published online by Cambridge University Press

Table VIII. Null space characteristics for one of the limiting poses with pose = [0.63m;0.66m;0.41m;29.2°;32.9°;28.7°] and linear acceleration {0 m/s^2; 0 m/s^2; 10 m/s^2}

Φ_1	Φ_2	Δ_1 (N)	Δ(a possible viable solution)(N)
0.462786	−0.04616	977.9386	4542.791
0.085282	0.594481	−2708.112	5787.304
0.484299	−0.02757	819.5860	4819.707
−0.19587	0.397983	−3345.05	65.74
0.436625	−0.08579	−1542.296	1271.95
−0.03853	0.440149	3420.889	8795.815
0.559601	0.224521	−728.68	7226.169
−0.01915	0.48354	3173.50	9286.897

any acceleration screw for all the poses required for the embodiment as a vehicle simulator (Table III and Table IV) (Fig. 12); it can potentially simulate impacts, which was difficult with traditional platforms because of the added inertia from actuators themselves.

7. Conclusion

The paper presents a methodology to improve the wrench closure workspace of CDPMs by perturbation of mounting points on the end-effector. It is shown that cable-suspended manipulators have a mathematical structure like robotics systems with multiple contacts. It is shown that a matrix affected by the configuration of mounting points on the end-effector and the fixed frame is responsible for the cable-driven parallel robot's behavior. A kinematics-based objective function has been proposed, inspired by the robotic systems with multiple contacts. The metric is used to optimize the cable attachment points on the end-effector.The proposed methodology has been shown to improve the CDPM's singularity-free workspaces for numerous test cases. A substantial increase of wrench closure workspace has been achieved (up to 30%) for traditional manipulators. The presented methodology has also removed the singularities of the manipulator within the workspace. A particular case is demonstrated where changing the mounting points on symmetrical cube-in-cube manipulators leads to a neat partitioning of the null space basis vectors near the manipulator's symmetric pose. The proposed method is also used to select the mounting points for a CDPM-based vehicle simulator.

Acknowledgements

The authors would like to acknowledge the Prime Minister's Research Fellowship (PMRF), Government of India for partially funding the research (to Rajesh Kumar).

Conflicts of Interest

The authors declare none.

References

1. A. Pott, *Cable-Driven Parallel Robots: Theory and Application* (Springer, New York, NY, USA, 2018).
2. A. Pott, H. Mütherich, W. Kraus, V. Schmidt, P. Miermeister and A. Verl, "IPAnema: A family of cable-driven parallel robots for industrial applications," *Mech. Mach. Sci.* **12**, 119–134 (2012).
3. S. Qian, B. Zi, W. W. Shang and Q. S. Xu, "A review on cable-driven parallel robots," *Chinese J. Mech. Eng.* **31**, 1–11 (2018), Article No. 66.
4. A. James, B. Roger and D. Nicholas, "The NIST robocrane," *J. Rob. Syst.* **10**(5), 709–724 (1993).
5. J. P. Sousa, C. G. Palop, E. Moreira, A. M. Pinto, J. Lima, P. Costa, P. Costa, G. Veiga and A. P. Moreira, "The SPIDERobot: A Cable-Robot System for On-Site Construction in Architecture," **In:** *Robotic Fabrication in Architecture, Art and Design* (2016) pp. 230–239.
6. T. Bruckmann, H. Mattern, A. Spengler, C. Reichert, A. Malkwitz and M. König, "Automated Construction of Masonry Buildings Using Cable-Driven Parallel Robots," *ISARC-Proceedings of the International Symposium on Automation and Robotics in Construction* (33) (2016).
7. G. Rosati, P. Gallina and S. Masiero, "Design, implementation and clinical tests of a wire-based robot for neurorehabilitation," *IEEE Trans. Neural Syst. Rehabilit. Eng*. **15**(4), 560–569 (2007).
8. Q. Chen, B. Zi, Z. Sun, Y. Li and Q. Xu, "Design and development of a new cable-driven parallel robot for waist rehabilitation," *IEEE/ASME Trans. Mech.* **24**(4), 1497–1507 (2019).

https://doi.org/10.1017/S0263574721000230 Published online by Cambridge University Press

9. E. Barnett and C. Gosselin, "Large-scale 3D printing with a cable-suspended robot," *Additive Manuf.* **7**, 27–44 (2015).
10. J. B. Izard, A. Dubor, P.E. Hervé, E. Cabay, D. Culla, M. Rodriguez and M. Barrado, "Large-scale 3D printing with cable-driven parallel robots," *Constr. Rob.* **1**(1), 69–76 (2017).
11. S. Qian, K. Bao, B. Zi and N. Wang, "Kinematic calibration of a cable-driven parallel robot for 3D printing," *Sensors* **18**(9), 2898 (2018).
12. I. Vukorep, "Autonomous Big-Scale Additive Manufacturing Using Cable-Driven Robots," *ISARC-Proceedings of the International Symposium on Automation and Robotics in Construction* (2017).
13. P. Bosscher, R. L. Williams and M. Tummino, "A Concept for Rapidly-Deployable Cable Robot Search and Rescue Systems," *ASME 2005 International Design Engineering Technical Conferences and Computers and Information in Engineering Conference* (2005) pp. 589–598.
14. R. L. Williams II, "Cable-suspended haptic interface," *Int. J. Virtual Reality*, **3**(3), 13–20 (1998).
15. J. V. Zitzewitz, G. Rauter, R. Steiner, A. Brunschweiler and R. Riener, "A Versatile Wire Robot Concept as a Haptic Interface for Sport Simulation," *IEEE International Conference on Robotics and Automation* (2009) pp. 313–318.
16. S. Qian, B. Zi, D. Wang and Y. Li, "Development of modular cable-driven parallel robotic systems," *IEEE Access* **7**, 5541–5553 (2018).
17. G. W. Brown, "Suspension system for supporting and conveying equipment, such as a Camera," U.S. Patent No. 4,710,819 (1987).
18. J. Rodnunsky and T. Bayliss, "Aerial cableway and method for filming subjects in Motion," U. S. Patent No. 5,224,426 (1993).
19. Z. Shao, T. Li, X. Tang, L. Tang and H. Deng, "Research on the dynamic trajectory of spatial cable-suspended parallel manipulators with actuation redundancy," *Mechatronics* **49**, 26–35 (2018).
20. S. Qian, K. Bao, B. Zi and W. D. Zhu, "Dynamic trajectory planning for a three degrees-of-freedom cable-driven parallel robot using quintic B-splines," *J. Mech. Des.* **142**(7), 073301-1–073301-13 (2020).
21. J. Begey, L. Cuvillon, M. Lesellier, M. Gouttefarde and J. Gangloff, "Dynamic control of parallel robots driven by flexible cables and actuated by position-controlled winches," *IEEE Trans. Rob.* **35**(1), 286–293 (2018).
22. R. J. Caverly and J. R. Forbes, "Flexible cable-driven parallel manipulator control: Maintaining positive cable tensions," *IEEE Trans. Control Syst. Technol*. **26**(5), 1874–1883 (2017).
23. H. Jamshidifar, S. Khosravani, B. Fidan and A. Khajepour, "Vibration decoupled modeling and robust control of redundant cable-driven parallel robots," *IEEE/ASME Trans. Mechatron*. **23**(2), 690–701 (2018).
24. G. Mottola, C. Gosselin and M. Carricato, "Dynamically feasible motions of a class of purely-translational cable-suspended parallel robots," *Mech. Mach. Theory* **132**, 193–206 (2019).
25. W. B. Lim, G. Yang, S. H. Yeo and S. K. Mustafa, "A generic force-closure analysis algorithm for cable-driven parallel manipulators," *Mech. Mach. Theory* **46**(9), 1265–1275 (2011).
26. S. R. Oh and S. K. Agrawal, "Cable suspended planar robots with redundant cables: Controllers with positive tensions," *IEEE Trans. Rob.* **21**(3), 457–465 (2005).
27. N. Zhang, W. Shang and S. Cong, "Geometry-based trajectory planning of a 3-3 cable-suspended parallel robot," *IEEE Trans. Rob.* **33**(2), 484–491 (2016).
28. K. Lakshminarayana, "Mechanics of Form Closure," ASME, 78-DET-32 (1978).
29. R. Verhoeven, M. Hiller and S. Tadokoro, "Workspace, Stiffness, Singularities, and Classification of Tendon-Driven Stewart Platforms," **In:** *Advances in Robot Kinematics: Analysis and Control* (1998) pp. 105–114.
30. K. Azizian, P. Cardou and B. Moore, "Classifying the boundaries of the Wrench-closure workspace of planar parallel cable-driven mechanisms by visual inspection," *ASME J. Mech. Rob.* **4**(2), 024503 (2012).
31. C. Pham, S. Yeo, G. Yang, M. Kurbanhusen and I. Chen, "Force-closure workspace analysis of cable-driven parallel mechanisms," *Mech. Mach. Theory* **41**(1), 53–69 (2006).
32. S. Bouchard, C. Gosselin and B. Moore, "On the ability of a cable-driven robot to generate a prescribed set of wrenches," *ASME J. Mech. Robot.* **2**(1), 011010 (2010).
33. P. Bosscher, A. Riechel and I. Ebert-Uphoff, "Wrench-feasible workspace generation for cable-driven robots," *IEEE Trans. Rob.* **22**(5), 890–902 (2006).
34. M. Gouttefarde, J. Merlet and D. Daney, "Determination of the Wrench-Closure Workspace of 6-DOF Parallel Cable-Driven Mechanisms," **In:** *Advances in Robot Kinematics* (2006) pp. 315–322.
35. X. Tang, W. Wang and L. Tang, "A geometrical workspace calculation method for cable-driven parallel manipulators on minimum tension condition", *Adv. Rob.* **30**(16), 1061–1071 (2016).
36. J. L. Pusey, A. Fattah, S. Agrawal, E. Messina and A. Jacoff, "Design and workspace analysis of a 6–6 cable-suspended parallel robot," *Mech. Mach. Theory* **39**(7), 761–778 (2004).
37. B. Ouyang and W. Shang, "Wrench-feasible workspace based optimization of the fixed and moving platforms for cable-driven parallel manipulators," *Rob. Comput. Integr. Manuf.* **30**(6), 629–635 (2014).
38. E. E. Hernandez, S. I. Valdez, M. Ceccarelli, A. Hernandez and S. Botello, "Design optimization of a cable-based parallel tracking system by using evolutionary algorithms," *Robotica* **33**(3), 599–610 (2015).
39. A. M. Hay and J. A. Snyman, "Optimization of a planar tendon-driven parallel manipulator for a maximal dextrous workspace," *Eng. Optim.* **37**(3), 217–236 (2005).
40. K. Azizian and P. Cardou, "The dimensional synthesis of planar parallel cable-driven mechanisms through convex relaxations," *J. Mech. Rob.* **4**(3), 031011 (2012).

https://doi.org/10.1017/S0263574721000230 Published online by Cambridge University Press

41. C. B. Pham, S. H. Yeo and G. Yang, "Workspace Analysis and Optimal Design of Cable-Driven Planar Parallel Manipulators," *IEEE Conference on Robotics, Automation and Mechatronics*, vol. 1, (2004) pp. 219–224.
42. K. Azizian and P. Cardou, "The dimensional synthesis of planar parallel cable-driven mechanisms through convex relaxations," *J. Mech. Rob.* **4**(3), 031011 (2012).
43. K. Azizian and P. Cardou, "The dimensional synthesis of spatial cable-driven parallel mechanisms," *J. Mech. Rob.* **5**(4), 044502 (2013).
44. M. Gouttefarde, S. Krut, O. Company, F. Pierrot and N. Ramdani, "On the Design of Fully Constrained Parallel Cable-Driven Robots," **In:** *Advances in Robot Kinematics (ARK)* (2008) pp. 71–78.
45. I. Hamida, M. Laribi, A. Mlika, L. Romdhane, S. Zeghloul and G. Carbone, "Multi-Objective optimal design of a cable driven parallel robot for rehabilitation tasks," *Mech. Mach. Theory* **156**, 104141 (2021).
46. X. Diao, "Singularity Analysis of Fully-Constrained Cable-Driven Parallel Robots with Seven Cables," *IEEE International Conference on Mechatronics and Automation (ICMA)* (2015).
47. S. Kawamura, H. Kino and C. Won, "High-speed manipulation by using parallel wire-driven robots," *Robotica* **18**(1), 13–21 (2000).
48. W. Lim, G. Yang, S. Yeo, S. Mustafa and I. Chen, "A Generic Tension-Closure Analysis Method for Fully-Constrained Cable-Driven Parallel Manipulators," *2009 IEEE International Conference on Robotics and Automation* (2009).
49. F. Dimentberg, *The Screw Calculus and its Applications in Mechanics* (Foreign Technology Div Wright-Pattersonafb, OH, 1968).
50. P. Miermeister, M. Lächele, R. Boss, C. Masone, C. Schenk, J. Tesch, M. Kerger, H. Teufel, A. Pott and H. H. Bülthoff, "The Cablerobot Simulator Large Scale Motion Platform Based on Cable Robot Technology," *2016 IEEE/RSJ International Conference on Intelligent Robots and Systems (IROS)* (2016) pp. 3024–3029.
51. T. Deter, A. Malczyk and M. Kuehn, "Validation of a Seat-Dummy Simulation Model for Rear-Impact," *20th International Technical Conference on the Enhanced Safety of Vehicles Conference (ESV)* (2007).
52. P. Tempel, P. E. Herve, O. Tempier, M. Gouttefarde and A. Pott, "Estimating Inertial Parameters of Suspended Cable-Driven Parallel Robots—Use Case on CoGiRo," *2017 IEEE International Conference on Robotics and Automation (ICRA)* (2017).
53. S. Sreenivasan, K. Waldron and S. Mukherjee, "Globally optimal force allocation in active mechanisms with four frictional contacts," *AMSE J. Mech. Des.* **118**(3), 353 (1996).
54. K. Usher, G. Winstanley and R. Carnie, "Air Vehicle Simulator: An Application for a Cable Array Robot," *Proceedings of the 2005 IEEE International Conference on Robotics and Automation* (2005).
55. E. Kljuno and R. Williams, "Vehicle simulation system: Controls and virtual-reality-based dynamics simulation," *J. Intell. Rob. Syst.* **52**(1), 79–99 (2008).
56. Motion Systems for a wide range of payload applications, http://www.moog.com/content/dam/moog/literature/ICD/Moog-Simulation-Motion_Systems-en.pdf, last modified 2015, accessed June 10, 2017.
57. V. Kumar and K. J. Waldron, "Force distribution in closed kinematic chains," *IEEE J. Rob. Autom.* **4**(6), 657–664 (1988).
58. Y. Zou, Y. Zhang and Y. Zhang, "On the Design of Singularity-Free Cable-Driven Parallel Mechanism Based on Grassmann Geometry," *ASME 2012 International Design Engineering Technical Conferences and Computers and Information in Engineering Conference* (American Society of Mechanical Engineers, 2012).
59. B. R. Zuo and W. H. Qian, "On the equivalence of internal and interaction forces in multifingered grasping," *IEEE Trans. Rob. Autom.* **15**(5), 934–941 (1999).

https://doi.org/10.1017/S0263574721000230 Published online by Cambridge University Press